Controlled Synthesis and Single-Particle Imaging of Bright, Sub-10 nm Lanthanide-Doped Upconverting Nanocrystals

Alexis D. Ostrowski, Emory M. Chan, Daniel J. Gargas, Elan M. Katz, Gang Han,[†] P. James Schuck, Delia J. Milliron, and Bruce E. Cohen*

The Molecular Foundry, Lawrence Berkeley National Laboratory, 1 Cyclotron Road, Berkeley, California 94720, United States. [†]Present address: Department of Biochemistry and Molecular Pharmacology, University of Massachusetts Medical School, Worcester, Massachusetts, United States.

ABSTRACT

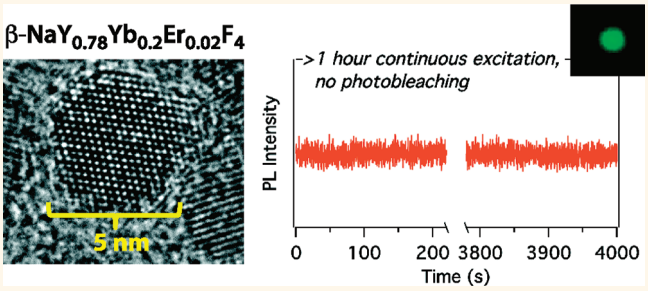

Phosphorescent nanocrystals that upconvert near-infrared light to emit at higher energies in the visible have shown promise as photostable, nonblinking, and background-free probes for biological imaging. However, synthetic control over upconverting nanocrystal size has been difficult, particularly for the brightest system, Yb^{3+}- and Er^{3+}-doped β-phase $NaYF_4$, for which there have been no reports of methods capable of producing sub-10 nm nanocrystals. Here we describe conditions for the controlled synthesis of protein-sized β-phase $NaYF_4$: 20% Yb^{3+}, 2% Er^{3+} nanocrystals, from 4.5 to 15 nm in diameter. The size of the nanocrystals was modulated by varying the concentration of basic surfactants, Y^{3+}:F^- ratio, and reaction temperature, variables that also affected their crystalline phase. Increased reaction times favor formation of the desired β-phase nanocrystals while having only a modest effect on nanocrystal size. Core/shell β-phase $NaYF_4$: 20% Yb^{3+}, 2% Er^{3+}/$NaYF_4$ nanoparticles less than 10 nm in total diameter exhibit higher luminescence quantum yields than comparable >25 nm diameter core nanoparticles. Single-particle imaging of 9 nm core/shell nanoparticles also demonstrates that they exhibit no measurable photobleaching or blinking. These results establish that small lanthanide-doped upconverting nanoparticles can be synthesized without sacrificing brightness or stability, and these sub-10 nm nanoparticles are ideally suited for single-particle imaging.

KEYWORDS: upconverting nanoparticles · lanthanides · phosphorescence · nanocrystal synthesis

Nanocrystals that have unusual or exceptional optical properties have shown promise as transformative probes for biological imaging.[1,2] A key requirement for use in bioimaging is that the nanocrystals be biocompatible, and for many experiments, this means that they need to be comparable in size to the biomolecules they are labeling, so as not to interfere with cellular systems.[3] Lanthanide-doped upconverting nanoparticles (UCNPs) are especially promising probes for single-particle tracking, but the synthesis of sub-10-nm β-$NaYF_4$, the crystal structure that hosts the most efficient upconversion, has not been reported, and questions remain about whether small β-$NaYF_4$ nanocrystals would retain the exceptional optical properties exhibited by larger UCNPs.

Synthetic methodologies that enable precise size control have been developed for several nanocrystals that have begun to find wider use in bioimaging, such as gold nanoparticles[4,5] and semiconductor quantum dots,[6,7] and these syntheses can produce nearly monodisperse nanocrystals in the size range (*ca.* 4−10 nm) of most membrane and globular proteins. Nanoparticles significantly larger than the biomolecules to which they are targeted may have limited accessibility to smaller subcellular structures, perturb trafficking patterns, retard diffusion, interfere with protein function or binding events, or alter pharmacokinetics.[8−10]

Synthetic methods for upconverting nanoparticles (UCNPs), which can be excited with continuous-wave (CW) 980 nm lasers and show upconverted phosphorescence at visible or NIR wavelengths,[11−16] have not been successful at producing bright nanocrystals less than 10 nm in diameter. β-Phase nanocrystals of $NaYF_4$ doped with lanthanide phosphors that have optical transitions in the visible region are especially promising for single-particle tracking experiments, as they show no measurable photobleaching or the luminescence intermittency (*i.e.*, blinking) exhibited by other probes, even over hours of continuous excitation.[17−20] We report here synthetic control over lanthanide-doped β-phase $NaYF_4$, down to 5 nm in diameter, and show that, like the >20 nm

* Address correspondence to becohen@lbl.gov.

Received for review January 6, 2012 and accepted February 16, 2012.

Published online February 16, 2012
10.1021/nn3000737

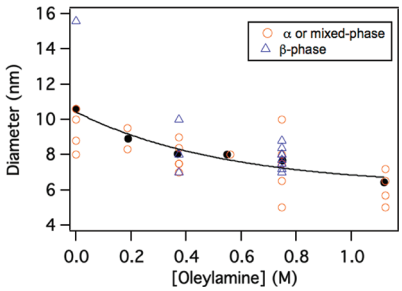

Figure 1. Effects of oleylamine on the size and phase of the $NaYF_4$:2% Er^{3+}, 20% Yb^{3+} nanocrystals, in 45 min 310 °C reactions, with sizes determined by dynamic light scattering. β-Phase nanoparticles are shown as blue triangles, α-phase or mixed phases as orange circles, and averages as closed black circles.

nanocrystals, single nanocrystals do not blink or photobleach. Addition of an undoped shell to the smaller nanocrystals leads to <10 nm nanocrystals with higher quantum yields than much larger UCNPs.

RESULTS AND DISCUSSION

Of the different UCNP nanocrystal matrices that have been reported, hexagonal β-phase $NaYF_4$ has been shown to have superior brightness compared to other compositions[2,21,22] and is 1−2 orders of magnitude brighter than comparable cubic α-$NaYF_4$.[11,23] Most β-phase $NaYF_4$ synthetic methods have reported a single size of nanoparticle in the 15 to 40 nm range, with good monodispersity but little apparent control over size.[14,24,25] Smaller UCNPs have included 7 nm lanthanide-doped $NaYF_4$ nanoparticles, but in the cubic α-phase,[12,26] 11 nm Yb−Tm-doped β-phase $NaYF_4$[24] and 11 nm Gd−Yb−Er−Tm-doped β-phase $NaYF_4$.[14,27,28] Our initial attempts to gain synthetic control over β-phase $NaYF_4$ nanocrystal size utilized a rare-earth trifluoroacetate (TFA) decomposition reaction, a two-step sequence that first produces α-phase nanocrystals that are then heated to 330 °C to form monodisperse 20−30 nm β-$NaYF_4$.[29] All attempts to isolate smaller β-phase nanocrystals from this scheme were unsuccessful, although eliminating oleic acid from the reaction did produce 10 nm β-$NaYF_4$ in the first step.[30] Unfortunately, these particles were strongly prone to aggregation and could not be transferred to water as individual nanocrystals.

Because TFA decomposition requires cleavage of a covalent bond to produce F^-, we reasoned that this may be inefficient at producing F^- and would limit nucleation,[31] leading to fewer, larger nanoparticles. As a more efficient F^- source, we combined NH_4F with oleylamine (OM)[32,33] and undertook a combinatorial screen varying reaction temperature, time, Y^{3+}:F^- ratio, Na^+ stoichiometry, and surfactant concentrations. In a typical reaction, rare-earth oleates were prepared from their chlorides and heated along with solid NH_4F, sodium oleate, and other surfactants in 1-octadecene to 300−330 °C (see Supporting Information for details).

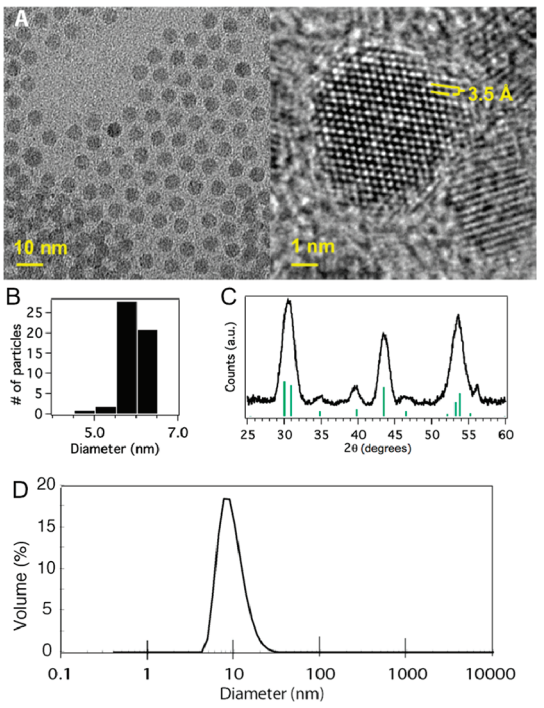

Figure 2. Characterization of the smallest UCNPs. (A) TEM images of the β-$NaYF_4$: 20% Yb^{3+}, 2% Er^{3+}. (B) Nanocrystal size distribution, measured by TEM (average particle diameter = 5.4 ± 0.6 nm; n = 50). (C) Powder XRD of 5 nm nanocrystals, with the β-$NaYF_4$ standard shown as green lines. (D) Size distribution of nanocrystals dispersed in hexane, measured by dynamic light scattering.

Reactions under these conditions produced either pure β-phase nanocrystals or mixtures of α- and β-phases.[34] Phase diagrams of bulk sodium yttrium fluoride suggest that β-phase formation is disfavored under most conditions, except a narrow window in which the 1:1:4 stoichiometry of Na^+, Y^{3+}, and F^- is strictly maintained.[35]

While previous reports have suggested that substoichiometric Y^{3+}:F^- ratios favor the formation of β-phase $NaYF_4$,[31,36] we found that, at reaction temperatures of 310 °C or higher, the 1:4 ratio was ideal for β-phase formation (Figure S2). We observed much stronger effects on nanocrystal size and phase by varying the composition of surfactants, with increasing oleylamine concentrations leading to smaller nanocrystals (Figure 1). The smallest β-$NaYF_4$ nanocrystals, 5 nm in diameter (Figure 2),[37] could be synthesized in 750 mM oleylamine at 310 °C, consistent with previous observations that oleylamine can modulate $NaYF_4$ size.[2,24]

In all of these reactions, we observed a trade-off between smaller size and β-phase formation, with higher temperatures favoring larger nanocrystals and consistent formation of the desired β-$NaYF_4$. Increasing oleylamine concentrations also favored the β-phase, allowing for lower reaction temperatures that produce smaller nanocrystals. Surprisingly, at the highest oleylamine concentrations at 310 °C, we observed mixed-phase reactions more often than at lower oleylamine concentrations (Figures 1 and S3).

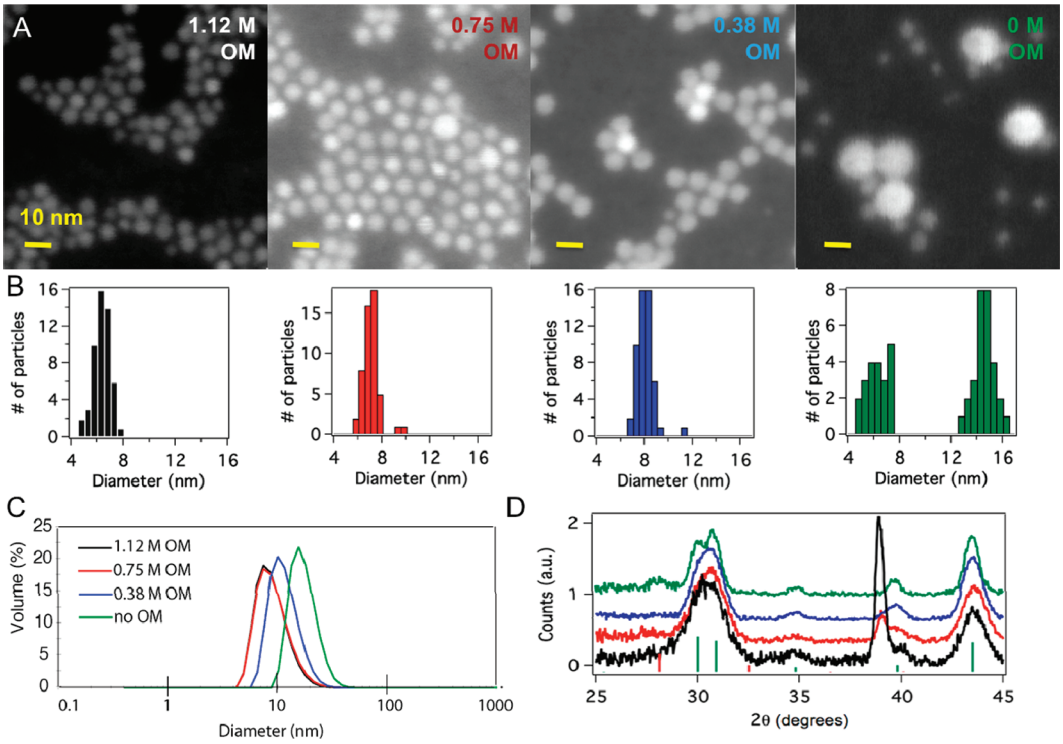

Figure 3. (A) Scanning transmission electron microscopy (STEM) images of representative β-$NaYF_4$ nanoparticle samples at different oleylamine concentrations of 1.12, 0.75, 0.38, and 0 M. Scale bar in each image is 10 nm. (B) Nanocrystal size distributions, measured by TEM (n = 50 for each). (C) Dynamic light scattering traces showing sizes as percent by volume. (D) Powder X-ray diffraction of as-prepared samples in (A). Peaks at 39° are NaF impurities.

This window of sub-10 nm β-$NaYF_4$ formation could be further refined with changes in reaction time. Increasing the reaction time from 15 to 60 min led to significant increases in the fraction of β-$NaYF_4$ in the presence of oleylamine (Figure S4a) but only small increases in nanoparticle diameter (Figure S4b). The increasing β-phase of the nanoparticles is also shown by an increase in the PL intensity with increasing reaction time (Figure S5). This increase in β-phase over time is suggestive of a direct α- to β-phase conversion facilitated by heat and oleylamine, although the nature of this transition is not known. We observed some variability in these conditions to consistently produce only β-phase $NaYF_4$, as determined by XRD, with some reactions yielding mixtures of α- and β-phases. The percentage of β-phase nanoparticles in the mixed-phase samples increases with addition of oleylamine up to 750 mM (Figure S3). At temperatures above 310 °C, the nanoparticles are increasingly β-phase (Figures S6 and S7), although this also increases the size of the nanocrystals for a given concentration of oleylamine (Figures 3 and 4). Given these constraints, we identified a window in which doped β-$NaYF_4$ could be prepared with diameters from 4.5 to 15 nm (Figures 3 and S6), and these particles are easily dispersed in organic solvents such as hexane or chloroform.

In studies using TFA precursors and similar [OM]:[OA] ratios to those used here,[30,38] either α-$NaYF_4$ or large (20−185 nm) β-$NaYF_4$ was reported. The comparison to this study is complicated by the limitations on stoichiometry imposed by use of TFA salts of Na^+ and RE^{3+}, and it is unclear in those methods how much F^- is actually being generated since the mechanisms of F^- liberation in these reactions are not well understood.

Oleylamine is likely to have indirect effects on size and phase in these syntheses, as recent work has shown that it efficiently condenses with oleic acid at temperatures ≥250 °C to form *N*-oleyloleamide (OOA).[39] IR and NMR analyses in these studies suggest that most or all of the OM should be consumed prior to nucleation if [OA] ≥ [OM], as is the case in all of these reactions (Figure 1). An NMR study examining interactions of these surfactants with the rare earth cations of nanocrystal surfaces found relative affinities of OA > OOA > OM,[39] suggesting a role for OOA in modulating nanocrystal size by weakening the coordination of RE^{3+} monomers. Monomer destabilization should lead to an increase in reactivity and enhanced nucleation, resulting in a larger number of smaller particles.

The role of oleylamine in the transition from α- to β-phase may be due to its consumption of OA, as previous work has found that OA favors α-$NaYF_4$ growth,[24,29,30] and under the conditions reported here, low [OM] almost exclusively favored α-$NaYF_4$ (Figure 1). IR and TEM studies have found a strong electrostatic interaction between oleate and the positively charged (100) planes of small α-NaYF4,[29] while density functional theory calculations have shown that the surface charges of α- and β-$NaYF_4$

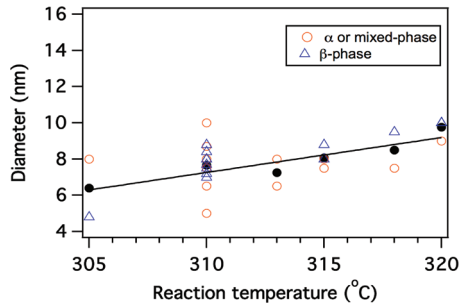

Figure 4. Dependence of $NaYF_4$ nanoparticle size and phase on reaction temperature, for 45 min reactions with 0.75 M oleylamine.

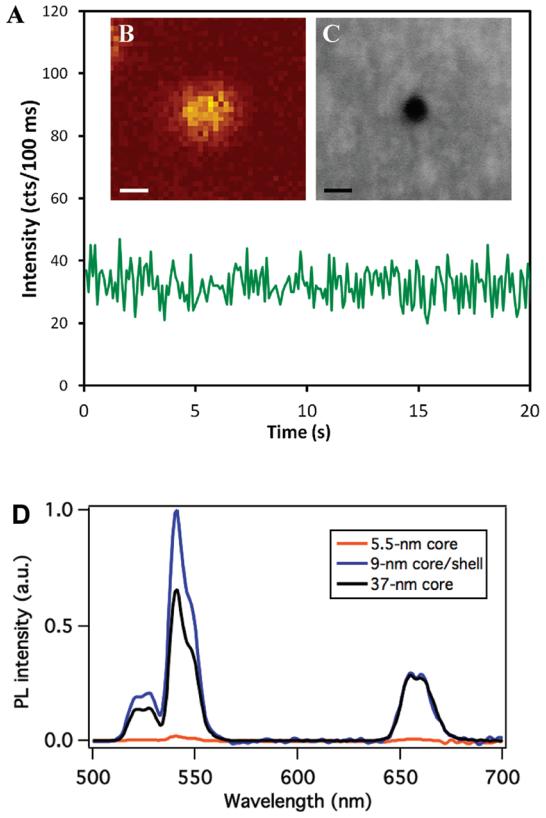

Figure 5. (A) Time-course plot of luminescence intensity from a single UCNP. (B) Confocal luminescence scan with 980 nm excitation. Scale bar is 500 nm. (C) SEM image of this nanocrystal. Scale bar is 10 nm. (D) PL intensities (λ_{ex} = 980 nm) of β-$NaYF_4$: 20% Yb^{3+}, 2% Er^{3+} nanocrystals in hexane compared to core/shells. Spectra are normalized to absorbance at 980 nm.

differ substantially.[14] This suggests that ligands of differing charge will promote different phases, and the neutral OOA will, like OM, favor the formation of β-$NaYF_4$. Unlike mechanistic studies of TFA-based synthesis of larger UCNPs, we do not see any evidence for dissolution of α-$NaYF_4$ in its transition to β-phase,[29] such as smaller α nanoparticles accompanying the β-$NaYF_4$ (Figures 2 and 3). In our mixed-phase reactions, we observe similarly broad XRD peaks for both α and β nanocrystals (Figures 2, 3, S1, S2, and S6), suggesting a phase change that proceeds without dissolution or dramatic changes in size.

We did observe that reducing the size of UCNPs cores reduced their brightness, a phenomenon that others have attributed to the coupling of a larger fraction of lanthanide activators to surface vibrational modes that promote nonradiative relaxation.[40] Previous work has shown that addition of a $NaYF_4$ shell without dopants increases the brightness and lifetime of UCNP phosphorescence.[41−44] A 2 nm shell was added to the 5 nm UCNPs, and the shell thickness was confirmed by TEM (Figure S9) and inductively coupled plasma elemental analysis (ICP) (Table S1). Optical characterization of these core/shell heterostructures confirms that the shell dramatically increases their brightness, conferring 50-fold higher quantum yields (QYs) compared to the 5 nm cores (Table S2). These heterostructures also do not photobleach or blink (Figures 5 and S9), and their emission is in fact larger than that of comparable 37 nm cores when normalized to the absorbance at 980 nm (Figure 5D).

While optimization of UCNP phase enhances their brightness, we questioned whether reducing their size would make them susceptible to photobleaching or blinking. Larger β-$NaYF_4$: 20% Yb^{3+}, 2% Er^{3+} nanocrystals (*ca.* 25 nm diameter) can withstand continuous 980 nm excitation at single-particle powers under ambient conditions for over an hour without any observable photobleaching or blinking, a remarkable stability for phosphors that may be due to the sequestration of a large fraction of the lanthanides within the $NaYF_4$ matrix.[18] Because phosphors exposed to air are prone to quenching, and the smaller nanocrystals have a much larger fraction of lanthanides at the nanocrystal surface, we examined whether they share the stability and continuous emission of the larger UCNPs.

Blinking from sub-10 nm core−shell UCNPs was investigated by confocal microscopy, in which UCNPs were dispersed onto SiN TEM grids and scanned with 980 nm excitation. Diffraction-limited spots of visible luminescence (Figure 5B) appear over the positions of single UCNPs, confirmed by STEM imaging (Figure 5C), and the intensity was plotted in 100 ms bin-times (Figure 5A). No intermittency is observed in the luminescence intensity from a single UCNP, suggesting that steady-state emission results from multiple Er^{3+} emitters in each UCNP. Resistance to photobleaching was examined during over an hour under continuous-wave 980 nm excitation at 10^6 W/cm^2, showing no degradation in UCNP emission (Figure S10). The small nanocrystals can be wrapped with an amphiphilic polymer to make them water-dispersible, showing only small changes in the effective hydrodynamic diameter (Figure S11) and emission intensity.[18]

The increased QY of the core/shell heterostructures likely arises from the dampening of high-energy vibrations originating at the surface by the 2 nm shells, which contain a sufficient number of unit cells (~4) of the low-phonon energy $NaYF_4$ lattice. The outermost 2 nm of a 37 nm core should also passivate the interior

of that nanocrystal, but we find that the 37 nm cores exhibit QYs about 20% lower than those of 9 nm core/shell heterostructures (Table S2). This suggests that energy excited in the Yb^{3+} sensitizers migrates rapidly *via* $Yb^{3+}-Yb^{3+}$ resonant energy transfer to the surface. These analyses demonstrate that synthetic control over UCNP size can enable the determination of critical length scales for vibrational quenching and energy migration in UCNPs.

CONCLUSION

We have used a combinatorial screen to identify reaction conditions that permit the synthesis of lanthanide-doped β-$NaYF_4$ nanocrystals with controlled diameters from 4.5 to 15 nm, which are comparable in size to many proteins, making them suitable for a variety of cellular imaging experiments. We find that nanocrystals less than 1/4 the diameter of previously characterized UCNPs retain their continuous emission and extreme resistance to photobleaching, and that 9 nm core/shell nanocrystals have higher quantum yields than >25 nm cores. These findings show that more biocompatible sizes of UCNP can be synthesized without sacrificing brightness or stability. Single particles of the core/shell heterostructures less than 10 nm in diameter were successfully imaged using a modest 980 nm CW laser as excitation source. This synthesis should be useful to produce nanocrystals to be used in extended single-molecule tracking experiments, as well as for novel lanthanide-doped nanocrystals with varying excitation and emission spectra that will be critical for multicolor upconverting imaging.

METHODS

Nanoparticle Synthesis. *Reagents.* Yttrium(III) chloride (anhydrous powder, 99.99%), ytterbium(III) chloride (anhydrous powder, 99.99%), and erbium(III) chloride (anhydrous powder, 99.9%) were purchased from Sigma-Aldrich and stored in a N_2 desiccator. Sodium oleate (Pfaltz and Bauer, 97%) was purchased from VWR. Anhydrous NH_4F was purchased from Sigma-Aldrich and stored under N_2. Oleic acid and 1-octadecene (tech. grade, 90%) were purchased from Sigma-Aldrich. Oleylamine (80−90%) was purchased from Acros.

Flask Synthesis of $NaYF_4$: 20% Yb, 2% Er. To a 50 mL round-bottom flask were added yttrium chloride (0.39 mmol, 76.1 mg), ytterbium chloride (0.1 mmol, 27.9 mg), and erbium chloride (0.01 mmol, 2.7 mg). Oleic acid (2.7 g), oleylamine (2 g), and 1-octadecene (3.5 g) were added. (For reactions without oleylamine, 5.5 g of 1-octadecene was added instead of 3.5 g.) The solution was stirred and then placed under vacuum and heated to 110 °C for 1 h. After 1 h, the reaction was brought under N_2. Solid sodium oleate (1.25 mmol, 380 mg) and anhydrous NH_4F (2 mmol, 74 mg) were added under N_2. The reaction was then heated to 310 °C. The reaction was stirred at 310 °C for 30 min to 1 h under N_2 and then cooled rapidly by a strong stream of air to the outside of the flask following removal of the heating mantle. When the reaction had cooled to 75 °C, absolute ethanol (9 mL) was added to the reaction solution to precipitate the $NaYF_4$: 20% Yb, 2% Er nanoparticles. The reaction was transferred to a centrifuge tube and allowed to cool to room temperature. The solution was centrifuged at 3000 *g* for 2−3 min to precipitate the nanoparticles completely. The supernatant was discarded, and the white solid (~80 mg) was suspended in minimal hexanes to break up the pellet. The nanoparticles where then precipitated again with addition of ethanol (~5 mL) and centrifuged at 3000*g* for 3 min. This washing procedure was repeated two more times to ensure washing of the reaction surfactants as well as any NaF impurities that were formed.

Optimized conditions to synthesize UCNPs of selected diameters are given in Table S3.

Automated (WANDA) Synthesis of $NaYF_4$:RE. A stock solution of rare-earth oleate was prepared, for Yb and Er-doped $NaYF_4$, by addition of yttrium chloride (3.51 mmol, 685 mg), ytterbium chloride (0.9 mmol, 252 mg), and erbium chloride (0.09 mmol, 25 mg) to a 100 mL round-bottom flask. Oleic acid (24.4 g) and 1-octadecene (14.2 g) were added. The suspension was stirred and then placed under vacuum and heated to 110 °C. After 1 h, the stock solution was cooled to room temperature and brought under N_2 in a glovebox equipped with the automated nanoparticle synthesis robot. To each reaction vial were added solid sodium oleate (1.25 mmol, 380 mg) and anhydrous NH_4F (2 mmol, 74 mg), followed by the rare-earth oleate stock solution (4.38 g) and oleylamine (0−10 mmol) and additional 1-octadecene (such that the total mass of ODE + OM = 5.5 g). The reaction vials were loaded onto the WANDA platform. The reactors were heated at 30 °C/min up to temperatures of 280−330 °C and held at that temperature for 30−60 min. The reactors were cooled to 75 °C, after which 9 mL of absolute ethanol was added to precipitate the nanoparticles. Aliquots were removed by the robot at appropriate time points and spotted into 96-well plates for either luminescence spectroscopy or XRD.

Synthesis of Core/Shell $NaREF_4/NaYF_4$. Undoped $NaYF_4$ shells were grown on the lanthanide-doped cores using a method modified from that of Abel *et al.*[44] YCl_3 was heated to 110 °C in oleic acid and ODE for 1 h. The solution was cooled to ~60 °C, and the stock solution of nanoparticle cores in hexane was added. The hexane was removed by vacuum, then the solution was cooled to room temperature after which NH_4F (2 mmol, 74 mg) and sodium oleate (1.25 mmol, 381 mg) were added. The solution was then heated to 280 °C for 30 min, then cooled rapidly, and 10 mL of ethanol was added when the solution reached <75 °C. Nanoparticles were precipitated and cleaned as described for the UCNP cores.

Characterization. *X-ray diffraction.* An aliquot (1 mL) of a stock solution of the nanoparticles in hexane was precipitated with addition of ethanol (~2 mL). The nanoparticle slurry was spotted onto glass coverslips or silicon wafers multiple times until an opaque white film formed. The sample was then allowed to air-dry completely. XRD patterns were obtained on a Bruker AXS D8 Discover GADDS X-ray diffractometer system with Cu Kα1 radiation (λ = 1.5406 Å) from 2θ of 15 to 65°.

For combinatorial screenings, the reaction mixture (250 μL) was spotted onto a glass crystallization plate (Symyx). The nanoparticles were precipitated from the reaction mixture onto the plate by addition of ethanol (~700 μL). The plate was centrifuged to concentrate the precipitated nanoparticles to the bottom of the wells. The supernatant was removed with a pipet and the plate dried in a vacuum desiccator overnight. XRD patterns were obtained on each sample directly on the glass plate from 2θ of 15 to 65°. The percentages of α- and β-phase $NaYF_4$ in each sample were determined by Rietveld refinement, by fitting the XRD patterns to α- and β-phase $NaYF_4$ in PANalytical X'Pert HiScore Plus software. Due to the peak broadening for the small nanocrystals, fittings of samples containing 8% or less of each phase appear identical to that of the pure phase.

Photoluminescence Spectroscopy. The emission spectra of the $NaYF_4$: 20% Yb, 2% Er nanoparticles were recorded on a

Horiba-Jobin Yvon Fluorolog II modified with a fiber-coupled 1 W continuous-wave 980 nm laser excitation source (Sheaumann) and a Micromax 96-well plate reader. The photoluminescence (PL) was measured in solid-state samples spotted onto either a clear polypropylene 96-well plate or onto a 96-well glass crystallization plate (Symyx).

For determination of PL quantum yields, the UCNP dispersions in hexane (500 μL) were placed in a quartz sample holder, which was inserted into an integrating sphere (Horiba Jobin-Yvon). The excitation laser to the integrating sphere and the emission to the Fluorolog II were routed using fiber optics. The excitation intensity was measured after passing through a 2.5% neutral density filter. For each sample, the emission was measured from 490 to 700 nm, with a band-pass of 5 nm and 1 s integration time. The excitation was measurement from 900 to 1000 nm with a band-pass of 5 nm and 1 s integration time. Each excitation and emission spectrum was measured three times. Blank samples of both emission and excitation were recorded between each sample to correct for time fluctuations in laser intensity. Excitation and emission spectra were corrected for the sensitivity of the detector over the appropriate wavelengths using a calibrated light source with the same integrating sphere, fiber optic setup, and detector.

The absolute quantum yield (QY) of each sample was then determined according to:

$$\Phi = \frac{(I_{em} - I_{blkem})}{(I_{ex} - I_{blkex})}$$

where I_{blkem} is the integrated intensity from 490 to 700 nm for the blank sample, I_{em} is the integrated intensity from 490 to 700 nm for the measurement sample, I_{blkex} is the integrated intensity from 900 to 1000 nm for the blank sample, and I_{ex} is the integrated intensity from 900 to 1000 nm for the measurement sample. Typical intensities of the sample excitation at 980 nm were ~10% less than those of blank intensities, indicating that the nanocrystals in the samples were absorbing only ~10% of the light. Values are reported as mean ± standard deviation.

Photostability measurements of UCNP photoluminescence were performed by exciting a thin film of UCNPs on a glass coverslip with a 980 nm continuous-wave laser (Thorlabs TCLDM9, 300 mW diode) at 10^6 W/cm^2. A high numerical-aperture objective (Nikon Plan Apo, 100×, 1.4 oil) was used to focus the laser and collect PL emission, which was then routed in free space to an avalanche photodiode (Micro Photon Devices, PDM series SPAD) for PL intensity measurements. A 750 nm short pass filter (Thorlabs) was used to filter residual excitation light after collection. The excitation density was determined from the measured laser power at the back aperture of the objective and the area of the focused excitation spot. PL intensity was recorded over 4000 s by a 1 MHz digital counter (RHK Technologies) measuring photon counts from the SPAD.

Confocal imaging of single upconverting nanoparticles was performed by dispersing dilute nanoparticle solutions (0.1 nM in hexane) onto SiN membrane TEM grids (Ted Pella #21569-10) and scanning with a 980 nm laser focused to a diffraction-limited spot by a 0.95 NA air objective (Zeiss). Luminescence from single nanoparticles was collected through the same objective and routed to an avalanche photodiode (Micro Photon Devices) for scanned image reconstruction by external software (RHK Technologies). Because the diffraction-limited beam spot is larger than individual nanoparticle size, single particles were confirmed on samples by subsequent SEM imaging operating in transmission mode. Intermittancy measurements of single-particle luminescence were performed by positioning the focused laser on a single particle and collecting the luminescence with 100 ms bin-times.

Lifetime Measurements. Time-resolved measurements of the PL emission from UCNPs were performed by modulating the excitation laser with a function generator (SRS, model DS340) connected to a voltage amplifier (SRS, model SIM983). The laser pulse edge and rep rate were 1 μs and 250 Hz, allowing a 2 ms window for PL decay. The measured photon counts from the SPAD and the trigger signal from the function generator were recorded simultaneously by a time-correlated single-photon counter (TCSPC) (PicoQuant, PicoHarp 300). The time arrival of PL emission referenced to laser pulse edge was calculated using a software program customized in MatLab.

Dynamic Light Scattering (DLS). The size of the nanocrystals was determined by DLS measurements on a Malvern Zetasizer. Samples were prepared from hexane stock solutions of the $NaYF_4$:20%Yb, 2%Er nanoparticles by dilution with hexane and filtered through a PTFE 0.2 μm syringe filter (Pall) into a quartz cuvette. The diameters of the nanoparticles in each sample were determined based on the fitting by volume. We note that we consistently found UCNP diameters determined by DLS to be *ca.* 2 nm larger than those determined by electron microscopy for the same samples, which most likely arises from the added hydrodynamic volume of surface ligands.

Electron Microscopy (STEM and TEM). For electron microscopy, dilute samples (7 μL) of nanoparticles in hexanes were dropped onto ultrathin carbon film/holey carbon, 400 mesh copper, or 300 mesh Au grids (Ted Pella). The grids were washed with ethanol and then hexanes. Images of the nanoparticles were obtained using a Zeiss Gemini Ultra-55 analytical scanning electron microscope. Dark-field images were collected in transmission (STEM) mode with 30 kV beam energy. TEM images were also obtained using a JEOL 2100-F 200 kV field-emission analytical transmission electron microscope. For single-particle determination, samples deposited on silicon nitride windows (Ted Pella) were used and imaged in STEM mode at 20 kV.

Elemental Analysis with ICP. The amounts of Na, Y, Yb, and Er in each sample were determined with ICP. Samples and standards were analyzed on a Varian 720-ES ICP optical emission spectrometer. Standards (Sigma Aldrich) were diluted in 7% HNO_3 to give standards with concentrations from 200 ppb to 5 ppm. Samples of UCNPs (1 mL of stock in hexane, ~5 mg/mL) were digested with concentrated HNO_3 (1−2 mL) and stirred with gentle heating (50 °C). The samples were then diluted by addition to 8 mL of water.

Conflict of Interest: The authors declare no competing financial interest.

Acknowledgment. We thank Dr. Virginia Altoe for help with electron microscopy. This work was supported by the Office of Science, Office of Basic Energy Sciences, of the U.S. Department of Energy under Contract No. DE-AC02-05CH11231.

Supporting Information Available: Additional characterization (STEM, XRD, PL spectra, quantum yields) of the nanoparticles. This material is available free of charge *via* the Internet at http://pubs.acs.org.

REFERENCES AND NOTES

1. Saint-Michel, E.; Giannone, G.; Choquet, D.; Thoumine, O. Neurexin/Neuroligin Interaction Kinetics Characterized by Counting Single Cell-Surface Attached Quantum Dots. *Biophys. J.* **2009**, *97*, 480–489.
2. Haase, M.; Schäfer, H. Upconverting Nanoparticles. *Angew. Chem., Int. Ed.* **2011**, *50*, 5808–5829.
3. Whitesides, G. M. The 'Right' Size in Nanobiotechnology. *Nat. Biotechnol.* **2003**, *21*, 1161–1165.
4. Brust, M.; Walker, M.; Bethell, D.; Schiffrin, D. J.; Whyman, R. Synthesis of Thiol-Derivatized Gold Nanoparticles in a 2-Phase Liquid−Liquid System. *Chem. Commun.* **1994**, *7*, 801–802.
5. Jun, Y. W.; Sheikholeslami, S.; Hostetter, D. R.; Tajon, C.; Craik, C. S.; Alivisatos, A. P. Continuous Imaging of Plasmon Rulers in Live Cells Reveals Early-Stage Caspase-3 Activation at the Single-Molecule Level. *Proc. Natl. Acad. Sci. U.S.A.* **2009**, *106*, 17735–17740.
6. Murray, C. B.; Norris, D. J.; Bawendi, M. G. Synthesis and Characterization of Nearly Monodisperse CdE (E = Sulfur, Selenium, Tellurium) Semiconductor Nanocrystallites. *J. Am. Chem. Soc.* **1993**, *115*, 8706–8715.
7. Peng, X.; Schlamp, M. C.; Kadavanich, A. V.; Alivisatos, A. P. Epitaxial Growth of Highly Luminescent CdSe/CdS Core/Shell Nanocrystals with Photostability and Electronic Accessibility. *J. Am. Chem. Soc.* **1997**, *119*, 7019–7029.
8. Lowe, A. R.; Siegel, J. J.; Kalab, P.; Siu, M.; Weis, K.; Liphardt, J. T. Selectivity Mechanism of the Nuclear Pore Complex Characterized by Single Cargo Tracking. *Nature* **2010**, *467*, 600–603.

9. Okuhata, Y. Delivery of Diagnostic Agents for Magnetic Resonance Imaging. *Adv. Drug Delivery Rev.* **1999**, *37*, 121–137.
10. Soo Choi, H.; Liu, W.; Misra, P.; Tanaka, E.; Zimmer, J. P.; Itty Ipe, B.; Bawendi, M. G.; Frangioni, J. V. Renal Clearance of Quantum Dots. *Nat. Biotechnol.* **2007**, *25*, 1165–1170.
11. Li, Z.; Zhang, Y.; Jiang, S. Multicolor Core/Shell-Structured Upconversion Fluorescent Nanoparticles. *Adv. Mater.* **2008**, *20*, 4765–4769.
12. Chen, G.; Ohulchanskyy, T. Y.; Kumar, R.; Ogren, H.; Prasad, P. N. Ultrasmall Monodisperse $NaYF_4$:Yb^{3+}/Tm^{3+} Nanocrystals with Enhanced Near-Infrared to Near-Infrared Upconversion Photoluminescence. *ACS Nano* **2010**, *4*, 3163–3168.
13. Shan, J.; Uddi, M.; Wei, R.; Yao, N.; Ju, Y. The Hidden Effects of Particle Shape and Criteria for Evaluating the Upconversion Luminescence of the Lanthanide Doped Nanophosphors. *J. Phys. Chem. C* **2010**, *114*, 2452–2461.
14. Wang, F.; Han, Y.; Lim, C. S.; Lu, Y.; Wang, J.; Xu, J.; Chen, H.; Zhang, C.; Hong, M.; Liu, X. Simultaneous Phase and Size Control of Upconversion Nanocrystals through Lanthanide Doping. *Nature* **2010**, *463*, 1061–1065.
15. Wang, F.; Wang, J. A.; Xu, J.; Xue, X. J.; Chen, H. Y.; Liu, X. G. Tunable Upconversion Emissions from Lanthanide-Doped Monodisperse-$NaYF_4$ Nanoparticles. *Spectrosc. Lett.* **2010**, *43*, 400–405.
16. Zhang, F.; Shi, Q.; Zhang, Y.; Shi, Y.; Ding, K.; Zhao, D.; Stucky, G. D. Fluorescence Upconversion Microbarcodes for Multiplexed Biological Detection: Nucleic Acid Encoding. *Adv. Mater.* **2011**, *23*, 3775–3779.
17. Nam, S. H.; Bae, Y. M.; Park, Y. I.; Kim, J. H.; Kim, H. M.; Choi, J. S.; Lee, K. T.; Hyeon, T.; Suh, Y. D. Long-Term Real-Time Tracking of Lanthanide Ion Doped Upconverting Nanoparticles in Living Cells. *Angew. Chem., Int. Ed.* **2011**, *50*, 6093–6097.
18. Wu, S. W.; Han, G.; Milliron, D. J.; Aloni, S.; Altoe, V.; Talapin, D. V.; Cohen, B. E.; Schuck, P. J. Non-blinking and Photostable Upconverted Luminescence from Single Lanthanide-Doped Nanocrystals. *Proc. Natl. Acad. Sci. U.S.A.* **2009**, *106*, 10917–10921.
19. Wang, F.; Banerjee, D.; Liu, Y. S.; Chen, X. Y.; Liu, X. G. Upconversion Nanoparticles in Biological Labeling, Imaging, and Therapy. *Analyst* **2010**, *135*, 1839–1854.
20. Park, Y. I.; Kim, J. H.; Lee, K. T.; Jeon, K. S.; Bin Na, H.; Yu, J. H.; Kim, H. M.; Lee, N.; Choi, S. H.; Baik, S. I.; *et al.* Nonblinking and Nonbleaching Upconverting Nanoparticles as an Optical Imaging Nanoprobe and T1 Magnetic Resonance Imaging Contrast Agent. *Adv. Mater.* **2009**, *21*, 4467–4471.
21. Kano, T.; Otomo, Y.; Yamamoto, H. $NaLnF_4$-Yb^{3+}, Er^{3+} (Ln-Y, Gd, La) - Efficient Green-Emitting Infrared-Excited Phosphors. *J. Electrochem. Soc.* **1972**, *119*, 1561–1564.
22. Shen, J.; Sun, L. D.; Yan, C. H. Luminescent Rare Earth Nanomaterials for Bioprobe Applications. *Dalton Trans.* **2008**, 5687–5697.
23. Qian, H. S.; Zhang, Y. Synthesis of Hexagonal-Phase Core—Shell $NaYF_4$ Nanocrystals with Tunable Upconversion Fluorescence. *Langmuir* **2008**, *24*, 12123–12125.
24. Yi, G. S.; Chow, G. M. Synthesis of Hexagonal-Phase $NaYF_4$: Yb,Er and $NaYF_4$:Yb,Tm Nanocrystals with Efficient Up-Conversion Fluorescence. *Adv. Funct. Mater.* **2006**, *16*, 2324–2329.
25. Zhang, F.; Li, J.; Shan, J.; Xu, L.; Zhao, D. Shape, Size, and Phase-Controlled Rare-Earth Fluoride Nanocrystals with Optical Up-Conversion Properties. *Chem.—Eur. J.* **2009**, *15*, 11010–11019.
26. Schietinger, S.; Menezes, L. d. S.; Lauritzen, B.; Benson, O. Observation of Size Dependence in Multicolor Upconversion in Single Yb^{3+}, Er^{3+} Codoped $NaYF_4$ Nanocrystals. *Nano Lett.* **2009**, *9*, 2477–2481.
27. Xiong, L. Q.; Yang, T. S.; Yang, Y.; Xu, C. J.; Li, F. Y. Long-Term *In Vivo* Biodistribution Imaging and Toxicity of Polyacrylic Acid-Coated Upconversion Nanophosphors. *Biomaterials* **2010**, *31*, 7078–7085.
28. Johnson, N. J. J.; Oakden, W.; Stanisz, G. J.; Scott Prosser, R.; van Veggel, F. C. J. M. Size-Tunable, Ultrasmall $NaGdF_4$ Nanoparticles: Insights into Their T1MRI Contrast Enhancement. *Chem. Mater.* **2011**, *23*, 3714–3722.
29. Mai, H. X.; Zhang, Y. W.; Si, R.; Yan, Z. G.; Sun, L. D.; You, L. P.; Yan, C. H. High-Quality Sodium Rare-Earth Fluoride Nanocrystals: Controlled Synthesis and Optical Properties. *J. Am. Chem. Soc.* **2006**, *128*, 6426–6436.
30. Chan, E. M.; Xu, C. X.; Mao, A. W.; Han, G.; Owen, J. S.; Cohen, B. E.; Milliron, D. J. Reproducible, High-Throughput Synthesis of Colloidal Nanocrystals for Optimization in Multidimensional Parameter Space. *Nano Lett.* **2010**, *10*, 1874–1885.
31. Ghosh, P.; Patra, A. Tuning of Crystal Phase and Luminescence Properties of Eu^{3+} Doped Sodium Yttrium Fluoride Nanocrystals. *J. Phys. Chem. C* **2008**, *112*, 3223–3231.
32. Xiong, L. Q.; Chen, Z. G.; Yu, M. X.; Li, F. Y.; Liu, C.; Huang, C. H. Synthesis, Characterization, and *In Vivo* Targeted Imaging of Amine-Functionalized Rare-Earth Up-Converting Nanophosphors. *Biomaterials* **2009**, *30*, 5592–5600.
33. Ryu, J.; Park, H.-Y.; Kim, K.; Kim, H.; Yoo, J. H.; Kang, M.; Im, K.; Grailhe, R.; Song, R. Facile Synthesis of Ultrasmall and Hexagonal $NaGdF_4$: Yb^{3+}, Er^{3+} Nanoparticles with Magnetic and Upconversion Imaging Properties. *J. Phys. Chem. C* **2010**, *114*, 21077–21082.
34. The percentages of α- and β-phase were determined by Rietveld fitting. Peak broadening for the smaller nanocrystals led to errors up to *ca.* 10% in fittings for samples containing <10% of a minor phase, as some intensities of the major phase overlap with and obscure those of the minor phase (Figure S1).
35. Thoma, R. E.; Hebert, G. M.; Insley, H.; Weaver, C. F. Phase Equilibria in the System Sodium Fuoride-Yttrium Fluoride. *Inorg. Chem.* **1963**, *2*, 1005–1012.
36. Wang, Z.; Tao, F.; Yao, L.; Cai, W.; Li, X. Selected Synthesis of Cubic and Hexagonal $NaYF_4$ Crystals *via* a Complex-Assisted Hydrothermal Route. *J. Cryst. Growth* **2006**, *290*, 296–300.
37. We observed that DLS consistently reported diameters *ca.* 2 nm larger than TEM or STEM for identical samples, presumably due to associated ligands and solvent in DLS measurements.
38. Mai, H.-X.; Zhang, Y.-W.; Sun, L.-D.; Yan, C.-H. Size- and Phase-Controlled Synthesis of Monodisperse $NaYF_4$: Yb, Er Nanocrystals from a Unique Delayed Nucleation Pathway Monitored with Upconversion Spectroscopy. *J. Phys. Chem. C* **2007**, *111*, 13730–13739.
39. Niu, W.; Wu, S.; Zhang, S. Utilizing the Amidation Reaction to Address the "Cooperative Effect" of Carboxylic Acid/Amine on the Size, Shape, and Multicolor Output of Fluoride Upconversion Nanoparticles. *J. Mater. Chem.* **2011**, *21*, 10894–10902.
40. Wang, F.; Wang, J.; Liu, X. Direct Evidence of a Surface Quenching Effect on Size-Dependent Luminescence of Upconversion Nanoparticles. *Angew. Chem., Int. Ed.* **2010**, *49*, 7456–7460.
41. Boyer, J. C.; van Veggel, F. Absolute Quantum Yield Measurements of Colloidal $NaYF_4$: Er^{3+}, Yb^{3+} Upconverting Nanoparticles. *Nanoscale* **2010**, *2*, 1417–1419.
42. Cui, X.; She, J.; Gao, C.; Cui, K.; Hou, C.; Wei, W.; Peng, B. Luminescent Properties of Nd^{3+}-Doped LaF_3 Core/Shell Nanoparticles with Enhanced Near Infrared (NIR) Emission. *Chem. Phys. Lett.* **2010**, *494*, 60–63.
43. Vetrone, F.; Naccache, R.; Mahalingam, V.; Morgan, C. G.; Capobianco, J. A. The Active-Core/Active-Shell Approach: A Strategy To Enhance the Upconversion Luminescence in Lanthanide-Doped Nanoparticles. *Adv. Funct. Mater.* **2009**, *19*, 2924–2929.
44. Abel, K. A.; Boyer, J.-C.; Andrei, C. M.; van Veggel, F. C. J. M. Analysis of the Shell Thickness Distribution on $NaYF_4$/$NaGdF_4$ Core/Shell Nanocrystals by EELS and EDS. *J Phys. Chem. Lett.* **2011**, *2*, 185–189.